IEEE Access
Multidisciplinary | Rapid Review | Open Access Journal

Received April 18, 2019, accepted May 15, 2019, date of publication May 27, 2019, date of current version June 11, 2019.

Digital Object Identifier 10.1109/ACCESS.2019.2919259

An Algorithm for the Computer Aided Design of Coil Couple for a Misalignment Tolerant Biomedical Inductive Powering Unit

ARSENY A. DANILOV[1,2], RAFAEL R. AUBAKIROV[1], EDUARD A. MINDUBAEV[1,2], (Member, IEEE), KONSTANTIN O. GUROV[1], DMITRY V. TELYSHEV[1,2], AND SERGEY V. SELISHCHEV[1], (Senior Member, IEEE)

[1]Institute of Biomedical Systems, National Research University of Electronic Technology, 124498 Zelenograd, Russia
[2]Institute for Bionic Technologies and Engineering, Sechenov First Moscow State Medical University, 119991 Moscow, Russia

Corresponding author: Arseny A. Danilov (arseny.danilov@gmail.com)

This work was supported by the Russian Science Foundation under Project 18-79-10008.

ABSTRACT Coils misalignments restrain the wider implementation of inductive powering of implantable medical devices. The misalignment problem can be overcome with the help of the coils geometry optimization. Coil couple design implies simultaneous adjustment of the several parameters (coils radii, turns numbers, and pitch). Thus, it is desirable to have the means for computer-aided design of the system. An algorithm for the coil couple design is devised. The key feature of the algorithm is the use of predefined maximum and minimum acceptable values of the load power as a performance metric. The algorithm gives the geometry of the coil which ensures that the inductive powering unit provides the given range of the load power for the given range of the misalignments. A formal method is proposed for the calculation of the initial coils characteristics and consequent adjustment of the transmitting coil external radius, transmitting coil turns number, coils internal radii (simultaneously), and receiving coil turns number. The software implementing the proposed algorithm was developed. Eight design runs were performed in order to evaluate the algorithm performance in various conditions, including different power ranges (10 W, 100 mW, and 300 μW), operating frequencies (0.2 MHz, 1 MHz, 6.78 MHz, and 13.56 MHz), and possible implementations (ventricular assist devices, cochlear implants, and spinal cord stimulators). It was proved that the power drop as low as 10% of the mean load power can be ensured for the lateral misalignments up to the receiving coil external radius. The low-power inductive powering unit was constructed and tested. The experimental results confirm the numerical modeling.

INDEX TERMS Electromagnetic coupling, inductive charging, inductive power transmission, implants.

I. INTRODUCTION

Wireless energy transfer for implantable medical devices (IMD) is a rapidly growing field of biomedical electronics [1]–[4]. Inductive powering represents the most popular solution among other wireless powering techniques such as energy harvesting or radiative energy transfer [5]–[8]. It is an established method of energy supply for cochlear implants [9], [10], and spinal cord stimulators [11], [12]. Prospective applications of this technique include powering of visual prostheses [13], cortical [14], and smart orthopedic implants [15], [16]. In addition, inductive powering of mechanical circulatory support systems is of special interest [17]–[20].

It can be said that inductive coils misalignments are one of the main restraints to wider implementation of IMDs wireless powering [3], [20], [21]. Changes in the tissue state and the patient activity can cause such misalignments, which, in its own turn, cause changes in the inductive powering unit (IPU) output characteristics [18], [20], [22]. At the same time, reliability and stability are one of the fundamental requirements for medical devices. Thus, significant efforts are dedicated to overcome the problem of the coils misalignment [20].

The associate editor coordinating the review of this manuscript and approving it for publication was Cihun-Siyong Gong.

Straightforward solutions imply using of means for restriction of the coils movements. For example, permanent magnets positioned at the coils centers are used in cochlear implants since 80's [23]. It is a feasible approach in the case of implants placed in a relatively immobile position (e.g., head). However, it does not provide enough rigidity if one needs to place the coils on a chest or an abdomen. In this case a dome-shaped casing of the implanted coil is used for a bulging of the patient skin [24]–[26]. The external coil is placed on top of the bulge, and adhesives can be used for fixation. This method is quite popular, but it has a serious drawback, because the shape of the external coil is greatly affected and it compromises the overall performance of the inductive link [20].

It is also possible to determine the position of the implanted coil with respect to position of the external coil and correct it manually [27]–[30]. It can be useful in the case of irregular misalignments caused by changes in the patient's body position (e.g., changing position from sitting to lying), but it is impossible to compensate effect of regular misalignments (caused, for example, by breathing) in such a way. Moreover, all direct approaches to the misalignment problem do not help to solve the problem of changes in the axial distance between coils. Therefore, there is a need for alternative or complimentary indirect compensation methods.

Indirect compensation of the misalignments can be performed in a wide variety of ways, but in most cases the strong coupling between the coils must be ensured. It leads to the frequency splitting phenomena, when IPU has two resonant frequencies (''odd'' and ''even'') instead of one and the values of those frequencies change with changing in coupling coefficient (coils position) [31], [32]. So-called ''stagger tuning'' was one of the first attempts to utilize frequency splitting to reduce sensitivity of the inductive link to the coils misalignment [33]. In this technique high coupling (overcoupling) of the coils must be ensured in order to provide stable voltage gain. High stability is obtained at the cost of the relatively low load power, and for this reason it is feasible solution only for the low-power IMDs (such as cochlear implants). Frequency tuning represents more flexible solution [34]–[37]. It implies adjustment of the IPU operating frequency to the ''odd'' (or seldom to the ''even'') splitting frequency according to the current coils position. In this manner, frequency tuning compensate misalignment effect and provide maximum load power for the given coils position. Interference with other radio-emitting devices is the main problem of this technique. In order to reduce the effect of the potential interference, IPU bandwidth should be kept as narrow as possible.

Optimization of the coils geometry is another option [38]–[41]. It was used in the first ever IMD, cardiac pacemaker, which was introduced in Sweden in 1958 and was equipped with an IPU for charging of the implanted batteries [38]. The charging was performed while sleeping and it was vitally important to have IPU with high misalignment tolerance. So, external (transmitting) coil has a much greater diameter than implanted one (25 and 5 cm respectively). It ensured the coupling between coils would be maintained at the cost of very low energy transfer efficiency. If one needs to use mobile (wearable) batteries, such a radical solution becomes impractical. Nevertheless, relatively big external coils are still in use. For example, in the IPU for the ReinHeart artificial heart system, the transmitting coil has an external diameter of 100 mm and the internal one of the 70 mm. Implanted coil has an external diameter of 70 mm. Lateral misalignments of up to 30 mm can be tolerated [39]. In other words, the IPU performs well when misalignments are less than the difference between external diameters of transmitting and receiving coils. Among these relatively simple approaches, more sophisticated methods for optimization of the coils geometry exist [40]–[42]. These methods usually include an adjustment of various coil characteristics such as fill factor (e.g., ratio of the internal radius of a coil to the external one) [40], [41], pitch or line width for the printed coils [41] and turns number [42].

Geometric optimization has its own limitations. First of all, size of the implanted receiver is restricted by medical considerations. The size of the external coil, in the case of the mobile devices with continuous powering, also should not exceed a certain value. Although constraints are much less rigid in this case. Finally, axial distance between coils is determined by the thickness of the skin and subcutaneous tissue. Thus, geometric optimization of an IPU cannot be considered a general solution. Nevertheless, it can be argued that the geometry of coils represents the single most important factor in the IPU design, because it directly affects the mutual and self-inductances, and, consequently, the coupling coefficient [41], [42]. Therefore, coils geometry optimization may be considered as a necessary first step in the IPU design process. If it is performed properly, sophisticated adaptation techniques such as a frequency tuning or an impedance matching can be incorporated in the final design more effectively.

It also should be mentioned that optimization of the coils geometry can be performed in a wide variety of ways by changing of the various parameters (external and internal diameters, turns number, pitch). Thus, it is desirable to have a formal design procedure which can be performed automatically [42]. In this paper, such a procedure is devised. It is based on the iterative adjustment of the coils geometric parameters to achieve desirable output characteristics (mean output power, acceptable power drop) in the given range of the coils displacements.

The paper is organized as follows. The mathematical model of the IPU is described in the Section II. The following section is devoted to the algorithm. Section IV demonstrates preliminary study of the algorithm and includes topics such as comparison of IPUs with optimized and non-optimized coil couple, assessment of the runtime performance of the algorithm, examination of the algorithm ability to compensate different types of misalignments and load resistances. Results of numerical modeling of IPUs with different output power and operating frequency are presented in Section V. Experimental verification of numerical modeling is described

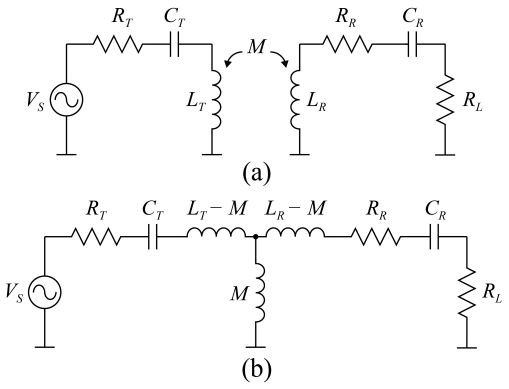

FIGURE 1. Equivalent model of an inductive powering unit (a) and T-equivalent representation of this model (b). Two inductively coupled LC-circuits are the basis of an IPU system.

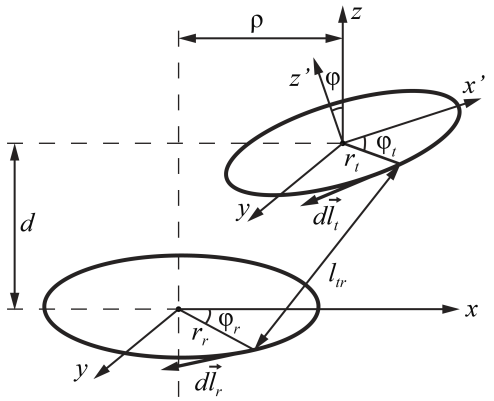

FIGURE 2. A pair of arbitrary oriented circular filaments that represent transmitting and receiving coils of an IPU. Changes in axial distance d, lateral distance ρ, and inclination φ displace the coils from an optimal position. This displacement can greatly affect performance of the IPU. Thus, geometric evaluation is essential for a proper IPU design.

in Section VI. Key findings and suggestions are discussed and summarized in Section VII.

II. MATHEMATICAL MODEL OF AN INDUCTIVE POWERING UNIT

In the following analysis an equivalent model of an IPU is considered represented by a pair of magnetically coupled LC-circuits (Fig. 1). Power source of the system is an ideal sine-wave generator. Operating frequency of the IPU ω_0 is equal to self-resonant frequencies of the LC-circuits in the transmitter and the receiver, L_T, L_R are self-inductances of the transmitting and receiving coil and C_T, C_R are compensating capacitances in the transmitting and receiving circuits. So-called series-series compensation architecture is used in this analysis. However, it should be noted that this algorithm may be implemented for other compensation types without major changes in the procedure.

The key performance metric of the IPU is load power which can be calculated using following expression:

$$P_L(M) = \frac{\omega_0^2 M^2 V_S^2 R_L}{\left(Z_T Z_R + \omega_0^2 M^2\right)^2}, \tag{1}$$

where R_L is a load resistance, V_S is a power source voltage, Z_T and Z_R are impedances of the receiving and transmitting parts of the system, and M is a mutual inductance between the coils. The mutual inductance function instead of a coupling coefficient function is chosen, because the mutual inductance can be derived directly from geometric considerations [33], [40]. Thus, a relationship between geometry of the coil couple and the load power can be established relatively easy by using expression (1) as long as the mutual inductance can be calculated.

The expression for a mutual inductance of a pair of arbitrary oriented circular filaments M_F (Fig.2) can be written as

$$M_F = \frac{\mu_0}{4\pi} r_t r_r \times \int_0^{2\pi}\int_0^{2\pi} \frac{(\cos\varphi_t \cos\varphi_r + \sin\varphi_t \sin\varphi_r \cos\varphi)}{l_{tr}} d\varphi_t d\varphi_r, \tag{2}$$

where φ is the angle between the filaments axes (angular misalignment), r_t, r_r are the radii of the filaments (radii of the transmitting and receiving coils windings), μ_0 is the magnetic permeability of a vacuum, and the distance between infinitely small section of the filaments l_{tr} can be expressed as

$$\begin{cases} l_{tr} = \sqrt{(x_t - x_r)^2 + (y_t - y_r)^2 + (z_t - z_r)^2} \\ x_t - x_r = \rho + r_t \cos\varphi_t \cos\varphi - r_t \cos\varphi_r \\ y_t - y_r = r_t \sin\varphi_t - r_r \sin\varphi_r \\ z_t - z_r = d + r_t \cos\varphi_t \sin\varphi, \end{cases} \tag{3}$$

where d is the axial distance between coil centers and ρ is the lateral one (lateral misalignment).

It should be mentioned that the presence of the conductive medium between the coils may affect the mutual inductance. Such effect can be incorporated in the Neumann's formula by multiplying equation (2) by relative magnetic permeability of the medium. However, biological tissues can be considered as diamagnetics ($\mu = 1$) for the frequencies of about 10 MHz and lower with high precision [43], [44].

Since there is no closed form expression for direct calculation of the mutual inductance, it is necessary to use numerical computation.

One can obtain expression for a mutual inductance of a coil couple M_C with turns number N and K [42]

$$M_C = \mu_0 \pi \sum_{i=1}^{N}\sum_{j=1}^{K} \frac{r_{t_i} r_{r_j}}{N_i K_j} \times \sum_{n_i=1}^{I_i}\sum_{k_j=1}^{J_j} \frac{\cos\varphi_{k_j}\cos\varphi_{n_i} + \sin\varphi_{k_j}\sin\varphi_{n_i}\cos\varphi}{l_{k_j n_i}}, \tag{4}$$

Equations (4) and (1) establish the relationship between the coils couple geometry and the load power. Therefore it can be said that (4) is a key formula for the algorithm. But, as long as coil geometry affects self-inductance, it is also

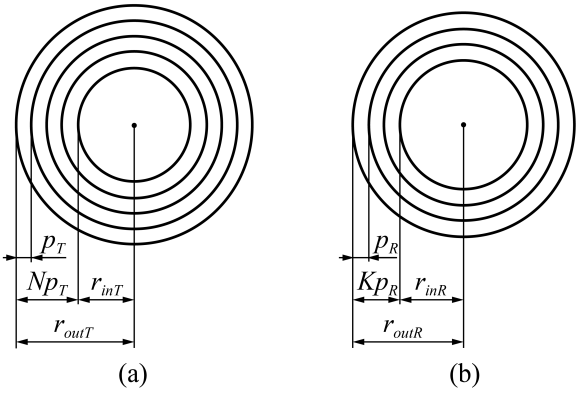

FIGURE 3. Schematic depiction of the transmitting (a) and receiving (b) coils. Flat circular coils are optimized in the proposed algorithm. Each coil is represented as a number of concentric circular wires. Parameters shown in this figure, namely, outer radius of the coils (r_{outT} and r_{outR}), inner radius of the coils (r_{inT} and r_{inR}), pitch (p_T and p_R) and number of turns (N and K) describe geometry of the transmitting and receiving coil.

necessary to take that influence into account. For that purpose the following equation can be used

$$L = \sum_{k=1}^{N} L_{turn} + \sum_{t=1}^{N} \sum_{i=1}^{N} M_{ti}, \quad i \neq t, \tag{5}$$

where the self-inductance of a single turn L_{turn} with a radius r can be expressed as

$$L_{turn} = \mu_0 r \left[\ln \frac{8r}{s} - \frac{7}{4} + \frac{s^2}{8r^2} \left(\ln \frac{8r}{s} + \frac{1}{3} \right) \right], \tag{6}$$

and s is a radius of the wire cross-section.

III. AN ALGORITHM FOR COIL COUPLE GEOMETRY OPTIMIZATION

The general idea of the devised algorithm can be summarized as follows: it performs an iterative adjustment of the coils geometric parameters (Fig. 3) to achieve preset values of maximum and minimum load power in the given range of the coils misalignments. The algorithm includes 11 steps described below. The flowchart is depicted on the Fig. 4. It should be mentioned here that the algorithm can be considered as a general algorithm for inductive systems with misaligned coils. The biomedical specific primarily is in the chosen coil sizes and operating frequency. The most important feature is the restriction of the receiving coil external radius (see Step I below). The effect of the tissue is not accounted for, and this assumption will be addressed in the Section VI.

STEP 1. ASSIGNMENT OF THE INITIAL VALUES

First of all, it is necessary to choose and define performance metrics of the system being optimized and design requirements. In the present case, the design performance metric is the range of the load power values for a given range of the misalignments. The boundaries of the load power range can be defined using preset required average output power P_L and

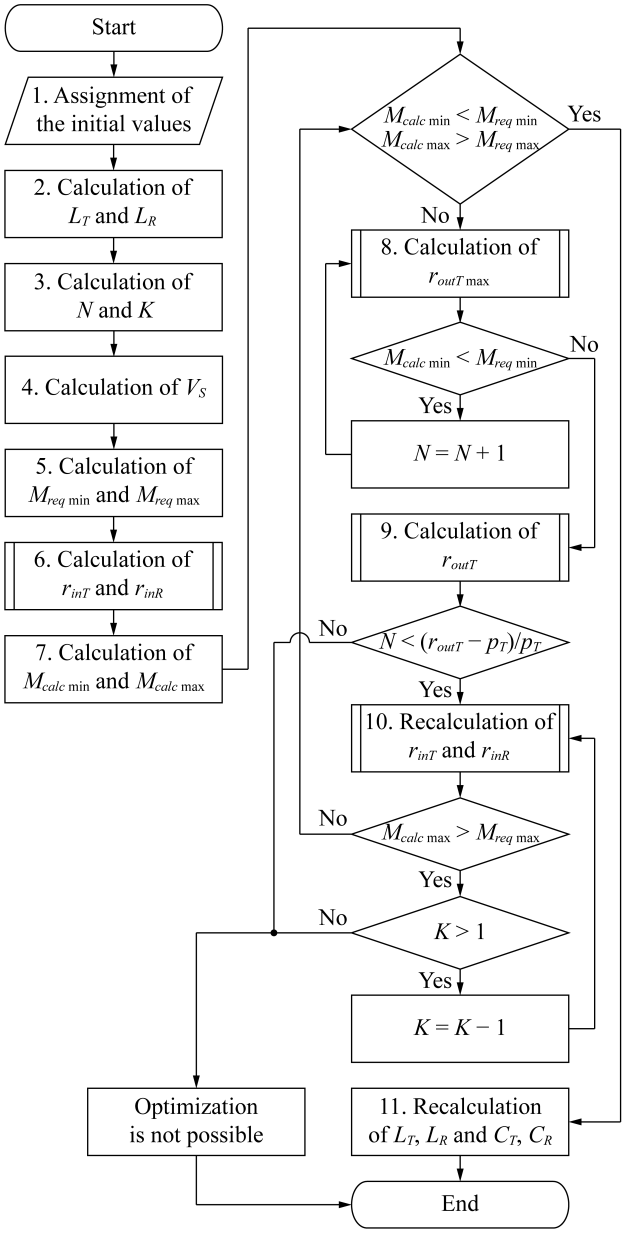

FIGURE 4. Flowchart of the proposed algorithm for coils couple geometry optimization in an IPU. The algorithm adjusts geometry of the coils to achieve preset values of maximum and minimum load power in the given range of misalignments between the coils.

acceptable power drop ΔP_L:

$$P_{Lreq\,\max} = P_L\,(1 + \Delta P_L), \tag{7}$$

$$P_{Lreq\,\min} = P_L\,(1 - \Delta P_L). \tag{8}$$

The design requirements are the given values of misalignments d, ρ, φ. At least one of these values must be set as a range, other two may be set as constants.

The design constants are the operating frequency ω_0 of the system and the load resistance R_L. The initial values of the capacitances C_{T0} and C_{R0} also should be set at this step. Values of these capacitors may change significantly as

a result of the design procedure. At this stage they can be guessed or chosen as technically feasible. This problem is discussed in more detail in the Section III.3.

The general aim of the procedure is coil couple geometry optimization. That is to say, coil parameters such as a number of coil turns, radii of turns and pitches for the transmitter and receiver should be adjusted to achieve desired performance metric. But, due to medical considerations, the outer radius of the receiver r_{outR} is strictly limited. Since the algorithm must provide stable output power, the radius r_{outR} must be set to the maximal possible value. This value should not be changed during the optimization procedure.

STEP 2. CALCULATION OF L_T AND L_R

The proposed procedure implies that the transmitting and receiving LC-circuits are tuned to the same resonant frequency equal to the operating frequency of the power source. Therefore, it is possible to calculate the self-inductances of the coils:

$$L_T = \frac{1}{C_{T0}\omega_0^2}, \tag{9}$$

$$L_R = \frac{1}{C_{R0}\omega_0^2}. \tag{10}$$

STEP 3. CALCULATION OF N AND K

After the first two preparatory steps it is possible to determine initial values of geometric parameters. Initial values for the external radius of the transmitting coil r_{outR}, the internal radii of the transmitting coil r_{inT}, and the receiving coil r_{inR} are set equal to the r_{outR} determined at the step 1:

$$r_{outT} = r_{imT} = r_{inR} = r_{outR}. \tag{11}$$

In other words, initially ideal identical coils with turns concentrated at the external radii is considered (the pitches in both coils are equal to zero). Then, the inductance of the single turn L_{turn} can be calculated using (6). As a result, the numbers of turns for the coils can be expressed as:

$$N = L_T/L_{turn}, \tag{12}$$

$$K = L_R/L_{turn}. \tag{13}$$

Since the turns number must be integer positive, the values of N and K are rounded up to the nearest integer.

STEP 4. CALCULATION OF V_S

The initial value of the source voltage V_S is calculated using (1):

$$V_S = \left(\frac{Z_T Z_R}{\omega_0 k_{crit}\sqrt{L_T L_R}} + \omega_0 k_{crit}\sqrt{L_T L_R}\right)\sqrt{\frac{P_{Lreq\,\max}}{R_L}}, \tag{14}$$

where k_{crit} is the critical coupling coefficient, which corresponds to the maximum possible value of load power for a given IPU, and can be expressed as

$$k_{crit} = \frac{1}{\sqrt{Q_T Q_R}}. \tag{15}$$

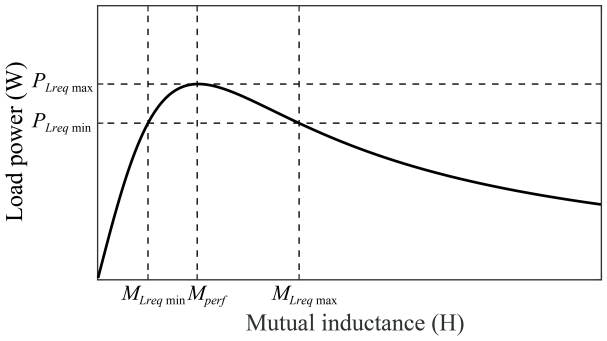

FIGURE 5. Mutual inductance between transmitting and receiving coils of an IPU. The IPU must be tuned for operation near critical coupling point. Boundary values of the IPU load power ($P_{Lreq\ max}$ and $P_{Lreq\ min}$) and corresponding required mutual inductance ($M_{req\ max}$ and $M_{req\ min}$) specify operating area of the IPU. The goal of the algorithm is to equate calculated (actual) boundaries of mutual inductance ($M_{calc\ max}$ and $M_{calc\ min}$) to the required values of the mutual inductance.

The Q_T and Q_R are the quality factors of the transmitting and the receiving parts of the IPU respectively:

$$Q_T = \frac{1}{R_T}\sqrt{\frac{L_T}{C_T}}, \tag{16}$$

$$Q_R = \frac{1}{R_L + R_R}\sqrt{\frac{L_R}{C_R}}. \tag{17}$$

The maximum value of the required load power $P_{Lreq\ max}$ is used instead of P_L since it expands the range of the mutual inductance values, in which the actual value of the load power lays between $P_{Lreq\ max}$ and $P_{Lreq\ min}$ (Fig. 5).

STEP 5. CALCULATION OF $M_{req\ min}$ AND $M_{req\ max}$

As can be seen from the Fig.5, a certain range of the mutual inductance values exists, in which the IPU provides required output power. Therefore, the main idea of the algorithm is to design a coil couple in such a way that the actual value of the mutual inductance is in this range for the all possible combinations of the coils misalignments.

The limits of the range of the mutual inductance values can be calculated as

$$M_{req\,\max} = \frac{V_S\sqrt{R_L} + \sqrt{V_S^2 R_L - 4P_{Lreq\,\min}Z_T Z_R}}{2\omega_0\sqrt{P_{Lreq\,\min}}}, \tag{18}$$

$$M_{req\,\min} = \frac{V_S\sqrt{R_L} - \sqrt{V_S^2 R_L - 4P_{Lreq\,\min}Z_T Z_R}}{2\omega_0\sqrt{P_{Lreq\,\min}}}. \tag{19}$$

Equations (18), (19) represent positive roots of a bi-quadratic equation, which can be derived from (1) by substituting $P_{Lreq\ min}$ for P_L.

STEP 6. CALCULATION OF R_{inT} AND R_{inR}

Now, it is possible to recalculate the internal radii of the coils, r_{inT} and r_{inR}, which were set as equal to the r_{outR} at the first step. The range of the physically possible values for r_{inR} is $[p_R, \ldots, r_{outR} - (K-1)p_R]$, where p_R is the pitch of the

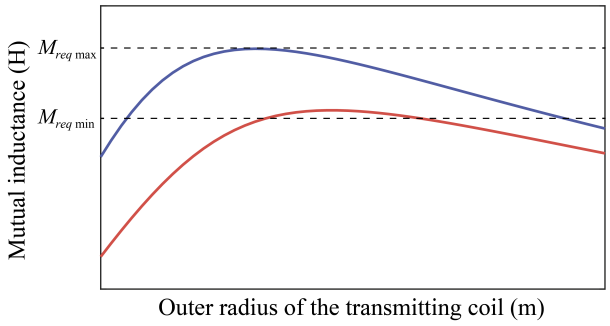

FIGURE 6. Minimal $M_{calc\ min}$ (red line) and maximal $M_{calc\ max}$ (blue line) values of the calculated mutual inductance as a function of the outer radius of the transmitting coil r_{outT}. The calculated mutual inductance changes nonmonotonically with changes in outer radius of the transmitting coil. The figure shows characteristic dependence, thus, no specific numbers are shown. $M_{req\ min}$ and $M_{req\ max}$ are shown with dashed lines.

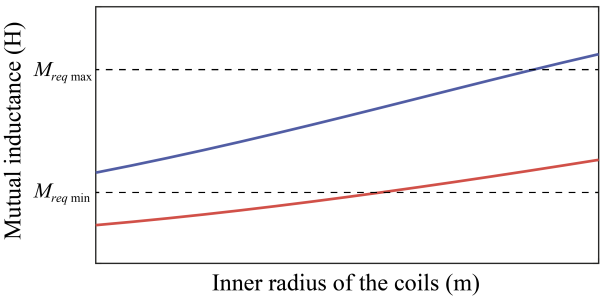

FIGURE 7. Minimal $M_{calc\ min}$ (red line) and maximal $M_{calc\ max}$ (blue line) values of the calculated mutual inductance as a function of the inner radius of the coils. The calculated mutual inductance changes monotonically with changes in inner radius of the coils. The figure shows characteristic dependence, thus, no specific numbers are shown. $M_{req\ min}$ and $M_{req\ max}$ are shown with dashed lines.

receiving coil (distance between turns). Similarly, for the r_{inT} it is $[p_T, \ldots, r_{outT} - (N-1)p_T]$, where p_T is the pitch of the transmitting coil. Thus, the values of the r_{inT} and the r_{inR} would be decreased and, accordingly, the maximum value of the mutual inductance would drop also. So, the r_{inT} and r_{inR} can be found by adjusting these values in such a way that the value $M_{calc\,max}$ calculated with the help of (4) will satisfy conditions $M_{calc\,max} \leq M_{req\ max}$ and $M_{calc\,max} \to M_{req\ max}$. It can be performed using bisection method.

STEP 7. CALCULATION OF $M_{calc\ min}$ AND $M_{calc\ max}$

The first design check can be performed after recalculation of the r_{inT} and r_{inR} values. The maximum and minimum values of the mutual inductance, $M_{calc\ min}$ and $M_{calc\,max}$, are calculated using new set of the coil geometric parameters for the given range of the misalignment values. If $M_{calc\,max} \leq M_{req\ max}$ and $M_{calc\ min} \geq M_{req\ min}$, then the main goal of the procedure is reached, and algorithm goes directly to the step 11. If it is not the case, a further iterative adjustment of the coils geometry is necessary.

STEP 8. CALCULATION OF $R_{outT\ max}$

If $M_{calc\ min} < M_{req\ min}$, the maximum necessary value of the external radius of the transmitting coil $r_{outT\ max}$ can be found by increasing the r_{outT} until $M_{calc\ min} \geq M_{req\ min}$. The dependence of the mutual inductance on the r_{outT} is nonmonotonic (Fig. 6). Thus, if increase of the r_{outT} leads to decrease of the $M_{calc\ min}$, the turns number of the transmitting coil must be increased as $N = N + 1$ without changes in the r_{outT}. Then the procedure of the gradual increasing of r_{outT} must be repeated.

STEP 9. CALCULATION OF R_{outT}

Calculation of the r_{outT} is performed in the same way as the calculation of the r_{inT} at the step 6. The range of the r_{outT} values is set as $r_{outT} = [r_{outR}, \ldots, r_{outR\ max}]$ and the iterative adjustment by the means of the bisection method are performed in order to achieve $M_{calc\ min} \geq M_{req\ min}$ and $M_{calc\ min} \to M_{req\ min}$.

After that, it is necessary to check the physical possibility of the fabrication of a coil with obtained parameters. If $N > (r_{outT} - p_T)/p_T$, the procedure must be terminated since the design of the IPU with the given parameters is impossible.

STEP 10. RECALCULATION OF R_{INT} AND R_{INR}

Then, it is necessary to change the value of the $M_{calc\,max}$ in such a way that it becomes less than or equal to $M_{req\ max}$. To this end the r_{inT} and r_{inR} can be recalculated using bisection method, similarly to the step 6. The range for the r_{inT} is $r_{inT} = [p_T, \ldots, r_{outT} - p_T]$. The range for the r_{inR} is $r_{inR} = [p_R, \ldots, r_{outR} - p_R]$.

The mutual inductance increases monotonically with the increase of the r_{inR} and the r_{inT} (Fig. 7). At the same time, the value of the internal radii is limited by the value of the external radii. Thus, when the upper limit of the range is reached, the number of turns for receiving coils should be decreased $K = K - 1$. If the $K = 1$, the optimization procedure must be terminated.

STEP 11. RECALCULATION OF L_T, L_R AND C_T, C_R

The geometry of the coils changes substantially in the course of the optimization procedure. Thus, it is necessary to reassess the coils self-inductances using (5). The values of the C_T and the C_R must also be recalculated:

$$C_T = \frac{1}{L_T \omega_0^2}, \tag{20}$$

$$C_R = \frac{1}{L_R \omega_0^2}. \tag{21}$$

This is the final step of the design procedure.

IV. PRELIMINARY STUDY OF THE ALGORITHM

In order to address some of the common issues, preliminary study of the algorithm was performed.

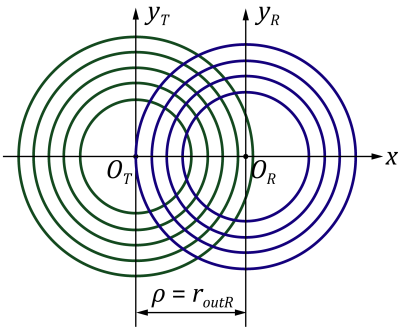

FIGURE 8. Depiction of relative position of the transmitting and receiving coils evaluated during the experimental verification of the algorithm: lateral displacement of the coils ρ changes from 0 mm to a value equal to outer radius of the transmitting coil r_{outR}. Axial distance d, and inclination φ are fixed.

A. COMPARISON OF OPTIMIZED AND NON-OPTIMIZED CASES

The comparison between optimized and non-optimized coil couples was performed in order to estimate how optimal is the geometry obtained with the help of the algorithm. The IPU with a couple of identical coils (non-optimized) was compared with the one which have optimized coil couple. It should be pointed out that there is no general approach for inductive coils design. The coils geometry for a non-optimized case was defined as follows: the turns number and the external radii of the coils were set equal to the turns number and external radius of the receiving coil in an optimized couple (15 and 35 mm respectively). The pitch was set equal to 1 mm. The P_L was set at 10 W, which can be considered suitable for VAD powering. The ΔP_L was chosen as 10%. Frequency $f_0 = \omega_0/2\pi$ was set at 200 kHz, and the initial capacitances C_{T0}, C_{R0} were chosen as 15 nF. The external radius of the receiver r_{outR} was equal to 35 mm as typical for VAD case [45]. The lateral misalignments were set in the range from 0 to 35 mm, and the angular misalignments were set equal to zero. In other words, the case when maximum value of the lateral misalignments is equal to the value of the external radius of the receiving coil was investigated (Fig. 8). It can be considered a boundary case, since the magnetic flux generated by the transmitting coil reaches a maximum at the axis of the transmitting coil. If $\rho_{\max} = r_{outR}$, the axis of the transmitting coil crosses the plane of the receiving coils at the outer extremes of the receiving coil. This case of optimized IPU will be referenced as "base case" later in the paper.

The results of the comparison of the optimized and non-optimized cases are depicted in the Fig. 9, and are summarized in the Table 1. It can be seen that for the IPU with non-optimized coil couple the power drop within selected range of lateral misalignments (0 . . . 35 mm) is about 7.7 W as against 2 W for the IPU with optimized coils couple. The output power of non-optimized IPU goes out of the required range at lateral misalignment 26 mm. At the same time, the IPU with optimized coils couple ensures the required load power level, 9 . . . 11 W, within selected lateral misalignment range, up to the 35 mm. It confirms the rational use of the

TABLE 1. Results of the algorithm implementation for inductive powering units with non-optimized (symmetrical) and optimized coils.

Value	Unit	Optimized (base case)	Non-optimized
Design requirements, constants and initial values			
P_L	W	10	10
ΔP_L	%	10	83.9
f_o	MHz	0.2	0.2
Results: transmitting circuits			
C_T	nF	34.1	36.6
L_T	µH	18.6	17.3
N		15	15
r_{outT}	mm	59.5	35
r_{inT}	mm	20.7	21
Results: receiving circuits			
C_R	nF	37.2	36.6
L_R	µH	17	17.3
K		15	15
r_{outR}	mm	35	35
r_{inR}	mm	20.7	21

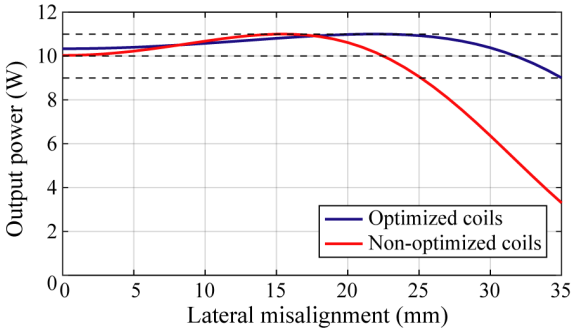

FIGURE 9. Load power of the IPU as a function of lateral misalignment for the IPU with coil couple optimized as a result of algorithm and non-optimized coils. The non-optimized coils geometry can be described as follows: the turns numbers and the external radii of the coils was set equal to the turns number and external radius of the receiving coil in an optimized couple (15 and 35 mm respectively), the pitch is 1 mm.

geometry of the coils. It should be pointed out that the algorithm provides coils geometry which ensures that the whole range of the possible mutual inductance would be covered (see Step 5, eq. (18) and (19)). Thus, the obtained solution strictly matched requirements for the load power drop within given misalignments range.

B. ASSESSMENT OF THE RUNTIME PERFORMANCE

The speed of the algorithm is another important issue that must be considered when feasibility of the algorithm is estimated. Relatively high discretization (I, J = 720, i.e. circle is approximated as a polygon with 720 sides) was used in the base case. The time lapse in this case is about 15 000 seconds. The time lapse this high can be considered as significant and even excessive. It must be mentioned that simple CPU computing (clock rate 3.6 GHz) was used instead of more complex and expensive GPU techniques presented in the authors earlier work [42]. Thus, the optimization run with lower discretization (I, J = 60) was performed to evaluate how the discretization affects the results and time

lapse. A considerable reduction in time lapse was noted: the solution took about 100 seconds. At the same time, difference in obtained values was minor, about 1-2% for the receiving coil inductance and receiving circuit capacitance, and even smaller for other values. The geometric parameters did not change at all, since the precision of the bisection method was less than loop discretization. All in all, it was found that the algorithm can be used with negligible time consumption for cases with the turns numbers of the order of 10.

C. COMPARISON BETWEEN DIFFERENT TYPES OF MISALIGNMENTS

The effect of different types of misalignments (i.e. axial, lateral and angular) was estimated in order to prove that the optimization algorithm can be used to compensate all types of misalignments. In this subsection the results for axial and angular misalignments are presented. The results for lateral misalignment of the coils are examined extensively in Section V.

The effect of angular misalignments was estimated in the following manner. The base case was set as a reference case and the optimization run was carried out for angular misalignments, which takes the maximum value equal to the 15 degrees in two opposite directions (inbound and outbound) for the fixed values of the $d = 0$ mm and $\rho = 0$ mm and $\rho = 35$ mm. It is very important to note that the values of the angular misalignments were taken as maximal physically possible in the given geometry. Similarly, estimation of the axial misalignments effect was performed. Two optimization runs was performed for axial misalignments in the range of $5 \ldots 15$ mm and $\rho = 35$ mm and $\rho = 0$ mm.

Results are summarized in the Table 2. It can be seen that angular misalignments affect the geometry of the transmitting coil slightly (r_{outT} is increased from 59.5 to 65.5 mm, N raised from 15 to 16) and the receiving coil does not change at all. Axial misalignments in the range $5 \ldots 15$ mm with the $\rho = 35$ mm also did not change results significantly in comparison with the base case. If $\rho = 0$ mm the resulting coil couples includes two identical coils which has geometry a very close to the geometry of the receiving coil in the base case. All in all, it can be said that lateral misalignments affects coils geometry much stronger than the angular and lateral ones. Thus, in what follows only lateral misalignment are considered in order to make the narrative more straightforward.

It should be mentioned here, that solutions provided by the algorithm can correspond to strong coupling as well as weak coupling between the coils. It can be seen from the Fig. 10 and Fig. 11. The monotonic curves correspond to the weak coupling, and curves with the local maximum correspond to the strong one.

D. ESTIMATION OF THE LOAD RESISTANCE EFFECTS

In order to access the effect of the different load resistance the base case was compared with three other cases with 100 and 200 Ohm load, and different initial capacitance and operating frequency (Table 3, Fig. 12). Size of the transmitting coil rises significantly in the 200 Ohm case with same initial load and frequency (up to 71-72 mm instead of 59.5 mm). Transmitting coil of this size can be considered impractical. Thus, we tested the case with higher operating frequency (0.8 MHz). The initial value of the C_{T0} and C_{R0} was also set as much lower than in previous cases (0.5 nF instead of 15 nF). As a result, the external radius of the transmitting coil drops significantly, to the value 49.5 mm.

TABLE 2. Comparison of results of the algorithm implementation for inductive powering unit for the angular and axial misalignments with the base case.

Value	Unit	Base case	Angular I (ρ=35 mm)	Angular II (ρ=0 mm)	Axial I (ρ=35 mm)	Axial II (ρ=0 mm)
Design requirements, constants and initial values						
P_L	W	10	10	10	10	10
ΔP_L	%	10	10	10	10	10
f_o	MHz	0.2	0.2	0.2	0.2	0.2
C_{T0}, C_{TR0}	nF	15	15	15	15	15
Results: transmitting circuits						
C_T	nF	34.1	28.8	37.2	34.4	45.4
L_T	μH	18.6	22.0	17	18.4	14.0
N		15	16	15	15	15
r_{outT}	mm	59.5	65.5	35	57.6	35
r_{inT}	mm	20.7	20.7	20.7	20.7	17.0
Results: receiving circuits						
C_R	nF	37.2	36.7	37.2	36.7	45.4
L_R	μH	17	17.2	17	17.2	14.0
K		15	15	15	15	15
r_{outR}	mm	35	35	35	35	35
r_{inR}	mm	20.7	20.7	20.7	20.7	16.9
Calculation parameters and performance data						
I, J		720	60	60	60	60
Time lapse	s	14 975	160	35	107	10

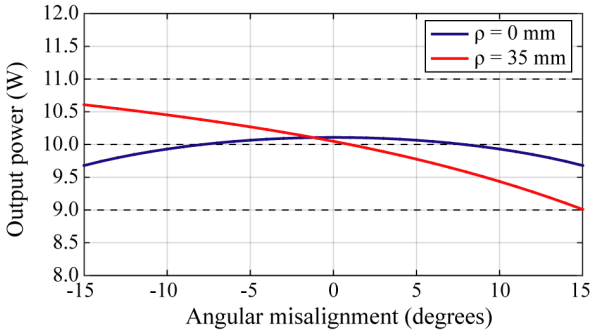

FIGURE 10. Load power of the IPU as a function of angular misalignment with the axial distance equal to 10 mm and two different values of the lateral misalignment: 0 mm (blue line) and 35 mm (red line).

V. NUMERICAL MODELING AND EXPERIMENTAL VERIFICATION

The software for the coil design using the proposed algorithm and MATLAB coding was developed. Eight different designs

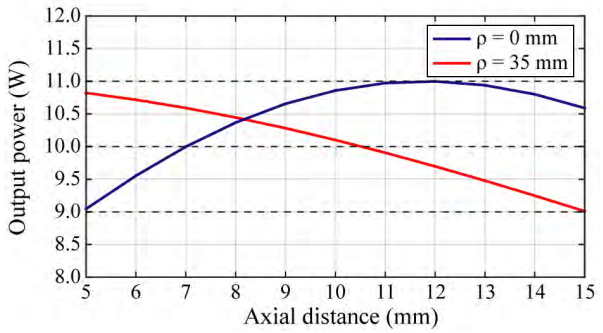

FIGURE 11. Load power of the IPU as a function of axial distance between the coils with angular misalignment equal to 0 degrees and two different values of the lateral misalignment: 0 mm (blue line) and 35 mm (red line).

TABLE 3. Comparison of results of the algorithm implementation for inductive powering unit for different load resistances and different initial capacitances and operating frequency.

Value	Unit	RL=20 Ohm	RL=100 Ohm	RL=200 Ohm	RL=200 Ohm
P_L	W	10	10	10	10
ΔP_L	%	10	10	10	10
f_o	MHz	0.2	0.2	0.2	0.8
C_{T0}, C_{TR0}	nF	15	15	15	0.5
Results: transmitting circuits					
C_T	nF	34.1	8.4	4.2	2.0
L_T	μH	18.6	75.1	151.2	19.4
N		15	29	41	20
r_{outT}	mm	59.5	71.4	71.0	56.3
r_{inT}	mm	20.7	20.7	20.7	6.2
Results: receiving circuits					
C_R	nF	37.2	36.7	36.7	2.9
L_R	μH	17	17.3	17.3	13.6
K		15	15	15	20
r_{outR}	mm	35	35	35	35
r_{inR}	mm	20.7	20.7	20.7	6.2
Calculation parameters and performance data					
I, J		720	60	60	60
Time lapse	s	14 975	944	2 115	290

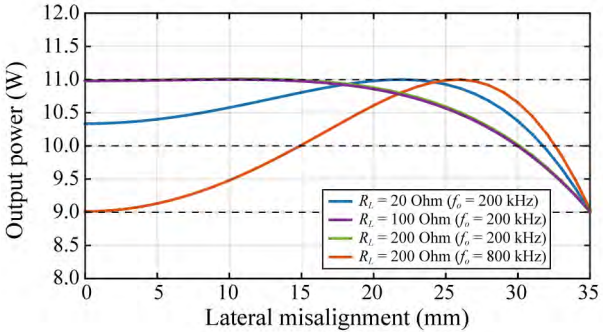

FIGURE 12. Load power of the IPU as a function of lateral misalignment between the coils with angular misalignment equal to 0 degrees for different load resistances, initial capacitances in the transmitter and receiver and operating frequencies.

of IPUs for various requirements were examined using the software to investigate the capabilities and restrictions of the algorithm. The main goals of the verification procedure were

TABLE 4. Results of the algorithm implementation for inductive powering unit in case of high-power application.

Value	Unit	Case I (base)	Case II
Design requirements, constants and initial values			
P_L	W	10	10
ΔP_L	%	10	10
f_o	MHz	0.2	10
C_{T0}, C_{R0}	nF	15	0.1
Results: transmitting circuits			
C_T	nF	34.1	0.31
L_T	μH	18.6	0.83
N		15	4
r_{outT}	mm	59.5	48.5
r_{inT}	mm	20.7	3.75
Results: receiving circuit			
C_R	nF	37.2	0.67
L_R	μH	17	0.38
K		15	3
r_{outR}	mm	35	35
r_{inR}	mm	20.7	3.75
Calculation parameters and performance data			
I, J		720	720
Time lapse	s	14 975	3 718

assessment of the effect of the operating frequency values, the ΔP_L requirements and the choice of C_{T0}, C_{R0} on the coils geometry and demonstration of the practicality of the proposed algorithm.

Eight case studies presented in what follows. In all cases the resistance of the receiving circuit was treated as negligibly low, the resistance of the transmitting circuit was set as 3 Ohm, and the load resistance was 20 Ohm. The axial distance between coils was set as equal to 10 mm. Different operating frequencies of IPU were modeled, both ISM (6.78 Mhz, 13.56 MHz) and non-ISM (0.2 MHz, 1 MHz), to test the developed algorithm.

A. HIGH-POWER APPLICATION

In the first two cases the high-power application of IPU was investigated.

In order to assess effect of the operating frequency on the coil size two cases were considered. In the first one $f_0 = \omega_0/2\pi$ was set at 200 kHz, and the initial capacitances C_{T0}, C_{R0} were chosen as 15 nF – this is the base case described in Section IV. In the second one $f_0 = \omega_0/2\pi$ was set at 10 MHz, and the initial capacitances C_{T0}, C_{R0} were chosen as 0.1 nF. It should be noted that such a relatively high operating frequency (10 MHz) is not feasible for the practical high-power application due to the possible tissue overheating. This value is chosen for demonstration purposes.

The algorithm provided a pair of significantly different LC-circuits designs (see Table 4). As was expected, for the high-frequency circuit transmitting coil is smaller (r_{outT} equal to 48.5 mm instead of 59.5 mm for a low-frequency circuit). There is also a significant difference in the r_{inT}/r_{inR} and the number of turns.

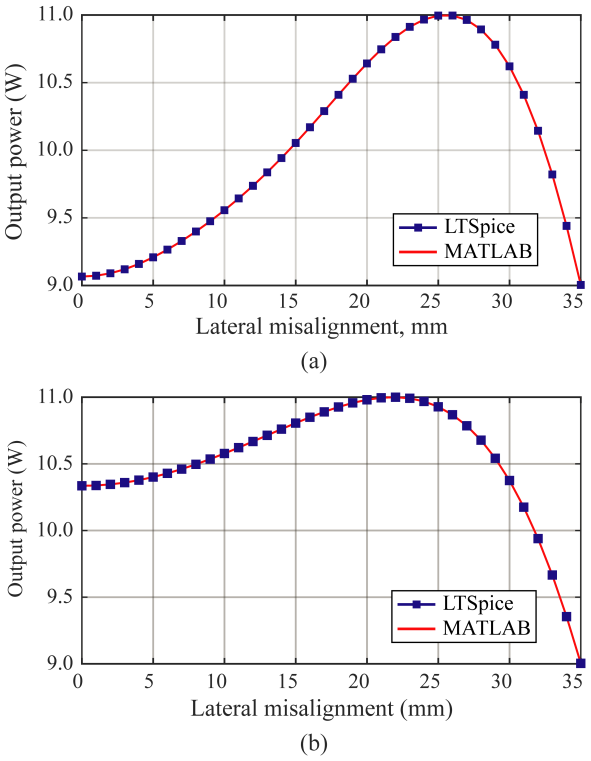

FIGURE 13. Load power of the IPU designed with the proposed algorithm as a function of lateral misalignment of the coils for Case I (a) and Case II (b). Corresponding parameters of IPUs are listed in the Table 4.

It was found that in both cases the values of the output power lie exactly in the defined range 9 . . . 11 W (Fig. 13). At the same time, for the lateral displacement in the range of 0 . . . 25 mm, the power drop for the high-frequency design is much higher (9 . . . 11 W), than for the low frequency design (10.4 . . . 11 W). In order to verify the calculations results were compared with LTSpice modeling. The results are in good agreement for MATLAB and LTSpice.

B. LOW-POWER/LOW-FREQUENCY CASE

In the second run two exemplary designs were developed for low-power/low-frequency cases in order to assess the influence of the ΔP_L requirements on the final design. The P_L was set as 0.01 W, the resonant frequency was chosen as 200 kHz and the C_{T0}, C_{R0} are set as equal to 15 nF. Relatively low frequency of 200 kHz is not usual for a low-power application. This value was chosen in order to provide in-depth assessment of the algorithm features. The values of misalignments, i.e. the resistances and the discretization parameters were similar to the Cases I, II. Two different requirements for a power drop ΔP_L were investigated, namely, 15% and more strict 10%.

Results of the algorithm implementation are summarized in the Table 5. First of all, it should be mentioned that the coils geometry for the Case III is similar to the Case II. In other words, the absolute value of the P_L did not affect calculation. Also, it can be seen that a significant difference in the

TABLE 5. Results of the algorithm implementation for inductive powering unit in case of low-power/low-frequency application.

Value	Unit	Case III	Case IV
Design requirements, constants and initial values			
P_L	W	0.01	0.01
ΔP_L	%	10	15
f_o	MHz	0.2	0.2
C_{T0}, C_{R0}	nF	15	15
Results: transmitting circuits			
C_T	nF	34.1	35.2
L_T	μH	18.6	18.0
N		15	15
r_{outT}	mm	59.5	54.4
r_{inT}	mm	20.7	20.7
Results: receiving circuit			
C_R	nF	37.2	37.2
L_R	μH	17.0	17.0
K		15	15
r_{outR}	mm	35	35
r_{inR}	mm	20.7	20.7
Calculation parameters and performance data			
I, J		720	720
Time lapse	s	14 579	13 398

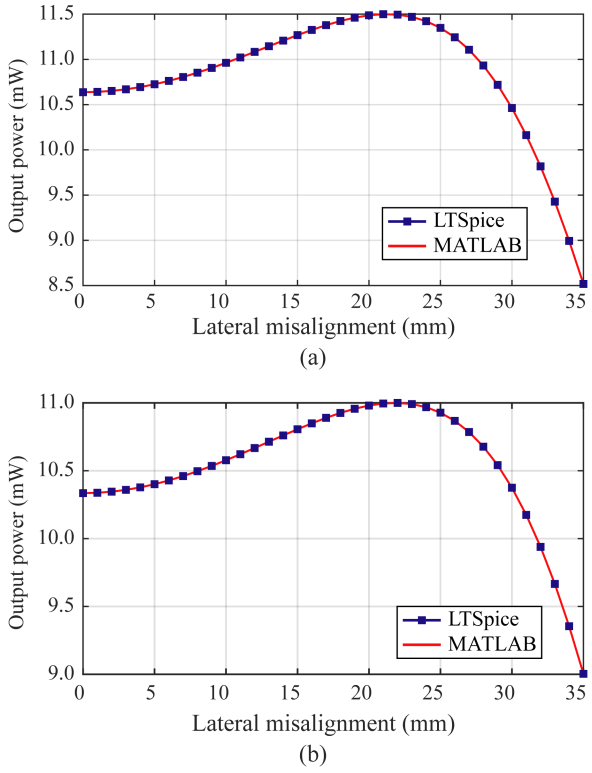

FIGURE 14. Load power of the IPU designed with the proposed algorithm as a function of lateral misalignment of the coils for Case III (a) and Case IV (b).

ΔP_L requirements leads to the minor difference in the transmitting coil geometry.

Fig. 14 depicts output characteristics of the IPU designed with the proposed algorithm as a function of lateral misalignment of the coils for Case III and Case IV. As in previous cases, the output power lies in the defined range, and the curves have smooth leading edges.

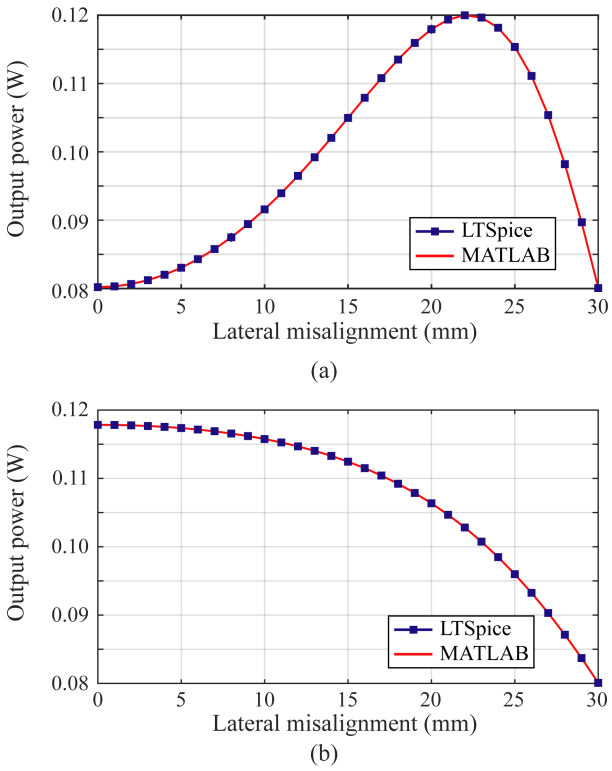

FIGURE 15. Load power of the IPU designed with the proposed algorithm as a function of lateral misalignment of the coils for Case V (a) and Case VI (b).

C. MID-POWER/MID-FREQUENCY CASE

As was mentioned in the section III, the choice of the C_{T0}, C_{R0} cannot be performed in the strict formal manner since it involves a number of different considerations. Nevertheless, it can be said that the simple choice between "large" and "small" values should be done at first. It is possible to estimate these ranges on the basis of achievable values of L_T, L_R and predefined value of f_o using (20), (21). In general, values of the order of 10 nF and higher can be considered "large", and values of about 1 nF and lesser can be considered as "small". Thus, two variants of the mid-power system were designed with C_{T0}, C_{R0} equal to 1 nF and 10 nF (Table 6). Output characteristics of the IPU designed with the proposed algorithm as a function of lateral misalignment of the coils for Case V and Case VI are presented on the Fig. 15.

The most significant result is the fact that in the Case VI IPU operates in the undercoupling mode for the whole range of lateral displacements. Moreover, the resulting design of the receiving coil is close to the physical limit since inner radius is nearly equal to the external one. Thus, taking into account results of the other case studies, it can be said, that initial values of capacitances for given soil sizes should be about 0.1 nF for frequencies in range of ∼10 MHz, ∼1 nF for ∼1MHz and ∼10 nF for 0.1 MHz.

D. MID-POWER/HIGH-FREQUENCY CASE

Finally, coil couples were designed using power consumption levels which can be considered typical for cochlear implants

TABLE 6. Results of the algorithm implementation for inductive powering unit in case of mid-power/mid-frequency application.

Value	Unit	Case V	Case VI
Design requirements, constants and initial values			
P_L	W	0.1	0.1
ΔP_L	%	20	20
f_o	MHz	1	1
C_{T0}, C_{R0}	nF	1	10
Results: transmitting circuits			
C_T	nF	4.51	5.13
L_T	μH	5.62	4.94
N		13	7
r_{outT}	mm	37.26	54.26
r_{inT}	mm	4.85	26.59
Results: receiving circuit			
C_R	nF	5.33	13.403
L_R	μH	4.75	1.89
K		13	4
r_{outR}	mm	30	30
r_{inR}	mm	4.85	26.59
Calculation parameters and performance data			
I, J		120	120
Time lapse	s	1 735	315

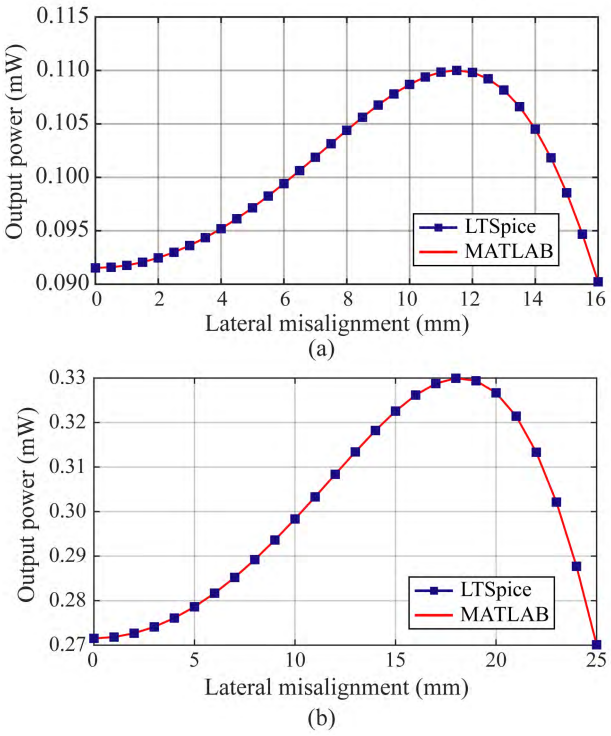

FIGURE 16. Load power of the IPU designed with the proposed algorithm as a function of lateral misalignment of the coils for Case VII (a) and Case VIII (b).

(Case VII) and spinal cord stimulators (Case VIII), standard operating frequencies (13.56 MHz and 6.78 MHz) and more strict size restrictions. Details are given in Table 7. Output characteristics are depicted at the Fig. 16.

The noticeable result is that coils were obtained with thinly distributed windings. It is also worth to mention that since the operating frequency lies in MHz-range, the power

TABLE 7. Results of the algorithm implementation for inductive powering unit in case of mid-power/high-frequency application.

Value	Unit	Case VII	Case VIII
Design requirements, constants and initial values			
P_L	W	0.1	0.3
ΔP_L	%	10	10
f_o	MHz	13.56	6.78
C_{T0}, C_{R0}	nF	0.1	0.1
Results: transmitting circuits			
C_T	nF	0.2	0.4
L_T	μH	0.6	1.6
N		5	7
r_{outT}	mm	20.9	35.9
r_{inT}	mm	4.8	3.3
Results: receiving circuit			
C_R	nF	0.3	1.3
L_R	μH	0.5	0.4
K		5	4
r_{outR}	mm	16	25
r_{inR}	mm	4.8	3.3
Calculation parameters and performance data			
I, J		720	720
Time lapse	s	1713	9132

drop is relatively high for $\rho = [0 \ldots 0.5 r_{outR}]$, similarly to the Case II.

VI. EXPERIMENTAL STUDY

For the experimental verification of the design procedure low-power case was chosen, with the P_L equal to the 300 μW. The ΔP_L was set as 20% and the operating frequency was chosen as equal to 1 MHz. The geometrical parameters of the coils are the same as in the case of numerical modeling: r_{outR} is 35 mm; d is 10 mm and ρ is in the range 0 . . . 35 mm.

The values of the resistances were chosen as in the previous cases. The C_{T0}, C_{R0} are chosen as equal to 1.5 nF.

Arbitrary function generator Tektronix AFG3252 was used to generate the alternating current driving the transmitting LC-circuit. Digital oscilloscope WaveRunner 8254R was used for the measurements.

The optimization procedure was carried out using developed software and the prototype IPU was constructed. Actual values of the IPU elements characteristics were slightly different from the calculated ones (see Table 8).

The coils were fabricated using 3D-printed frames (Fig. 17). It should be noted that in the above mentioned formulas for self- and mutual inductance calculation coils are approximated as a set of ideal rings. In the fabricated coils there are jumpers between turns, therefore, a slight difference exist in the self- and mutual inductance of the modeled and fabricated coils.

The verification of the results was performed in the following manner. The calculated values from Table 5 were used for calculation of the dependence of the P_L on the ρ using (1) and (4). It was compared with LTSpice simulation with the actual values of the IPU components including equivalent series resistance (ESR) of the coils, as well as with the components without ESR (Fig. 18). It was found that the results of

TABLE 8. Calculated and actual values of the designed IPU.

Parameter	Dimension	Calculated	Actual
Transmitting circuit			
Outer radius of the coil, r_{outT}	mm	42.9	43
Inner radius of the coil, r_{inT}	mm	15.3	15
Number of turns in the coil, N		9	9
Self-inductance of the coil, L_T	μH	4.90	4.90
Compensating capacitance, C_T	nF	5.17	5.2
Receiving circuit			
Outer radius of the coil, r_{outR}	mm	35	35
Inner radius of the coil, r_{inR}	mm	15.3	15
Number of turns in the coil, K		9	9
Self-inductance of the coil, L_R	μH	4.58	4.6
Compensating capacitance, C_R	nF	5.53	5.62

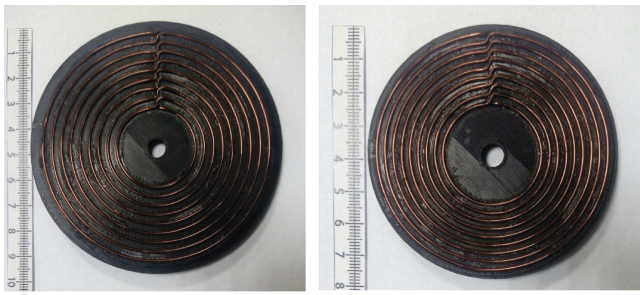

(a) (b)

FIGURE 17. Transmitting (a) and receiving (b) coils fabricated for the experimental studies. Parameters of the coils are listed in Table 2.

the MATLAB and LTSpice simulation that does not account for ESR of the components are in very close agreement. The experimental curve lays little bit lower than calculated. It can be attributed to the parasitic effects not taken into account in the course of the optimization. Another possible explanation is a slight difference between the geometrical parameters given by the algorithm and the geometrical parameters of the manufactured coils (see Table 8). Nevertheless, the general aim of the optimization procedure was achieved, since the ΔP_L was a little bit lower than the target value (18.6% instead of 20%) and the value of the P_L was inside the target range for the lateral misalignments in the range of 5 . . . 34 mm.

Additionally, effect of biological tissue on the output power of the IPU was measured. Transmitting and receiving coils were separated by porcine meat. Results of the measurements are presented in Fig. 18. It can be concluded that for the given tissue thickness and frequencies only a small difference (about 1 . . . 3%) in output power is present for energy transfer through air and porcine meat.

The effect of the alterations in the axial distance on the IPU performance was assessed. Two cases were considered, for the actual value of the axial distance which is lower (8 mm) and higher (12 mm) than nominal. For the both cases MATLAB and LTSpice curves are in good agreement and the experimental value of the load power was lower than calculated.

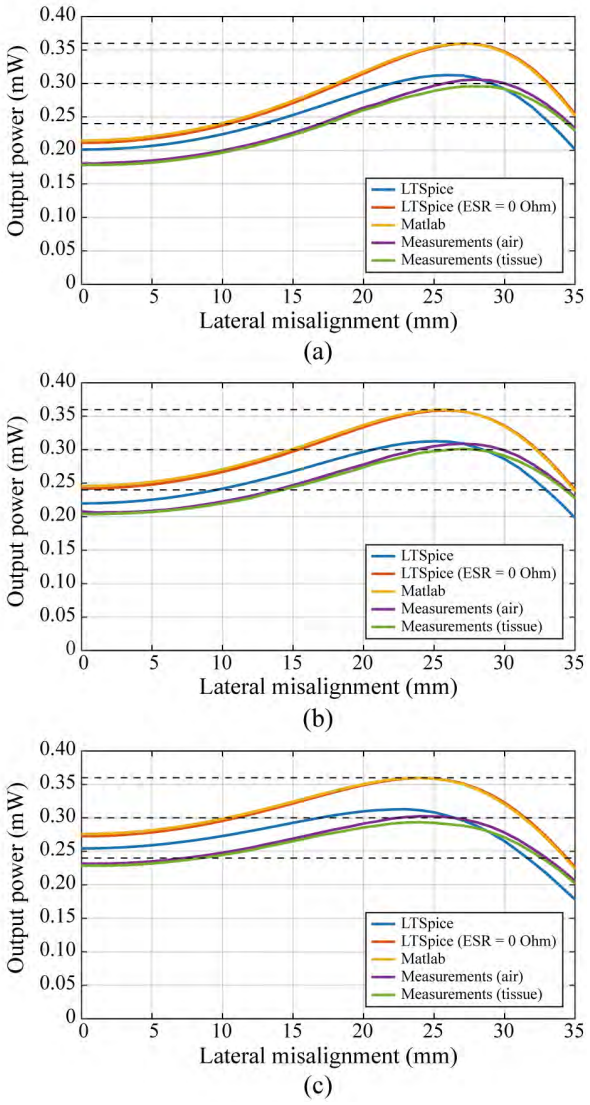

FIGURE 18. Load power of the IPU as a function of lateral misalignments obtained experimentally in the air (purple line) and in the biological tissue (green line), using LTSpice simulation with actual values of the IPU elements (blue line) and LTSpice simulation that did not account for ESR of the components (red line) and using MATLAB calculation with the calculated values (orange line). Results are obtained for the axial distance equal to the 8 mm (a), 10 mm (b) and 12 mm (c). The parameters of the IPU are listed in Table 5.

The decrease of the axial distance leads to the significant changes in the load power level, which is lower than required for the ρ in the range of $0 \ldots 12$ mm. For the increasing axial distance situation is quite opposite, the load power are inside the acceptable range for the most part of the lateral misalignments range and is lower than required only for relatively high ρ, it is $34 \ldots 35$ mm.

It can be explained in the following manner: the performance of the IPU depends on the coupling coefficient k, which must be kept inside specific range in order to provide the required load power. For this case the k must lay between 0.14 and 0.49. Equipotential curves were calculated for k in dependence of the lateral and axial distance (Fig. 19). It can

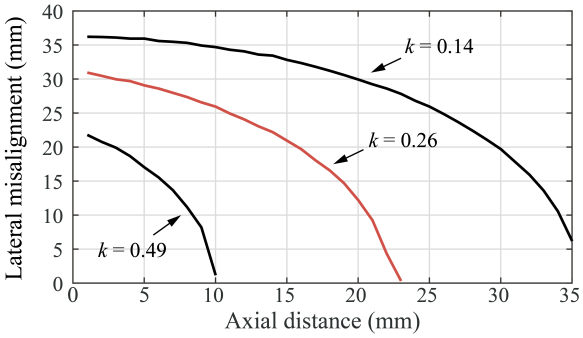

FIGURE 19. The ratio of the axial distance and the maximum lateral misalignments at which the required output power is provided (black lines depict values of coupling coefficient corresponding to the limit of the coils misalignments, red line depicts values of misalignments at which a critical coupling is provided).

be seen that the coupling coefficient is kept constant when decreasing of the axial distance corresponds to the increasing of the lateral misalignments and vice versa. Thus, if the design procedure is performed for constant axial distance and the range of lateral misalignments (which is preferable from the time-cost point of view), the axial distance must be chosen as a minimal possible instead of the expected mean value. The maximal value of the lateral misalignment should be set slightly more than the expected one.

VII. CONCLUSION

In this paper, the algorithm for coil couple geometry optimization was devised to achieve desirable stability of the output characteristics of the IPU. The distinctive feature of the algorithm is that the output power drop in the IPU is used as a performance metric. It is also important that the proposed design procedure is strictly formal. Therefore, this procedure can be fully implemented as software. Therefore, the algorithm can be used for computer-aided design of IPUs.

Comprehensive numerical analysis of the capabilities and restrictions of the algorithm was performed. The practicable solutions were obtained for the power drop as small as 10%, and the lateral misalignments up to the value of the external radius of the receiving coil ($\rho = r_{outR}$). Experimental verification was performed for the power drop of 20%. It also was found that output characteristics change slightly due to correction of the coils geometric characteristics (i.e., rounding of the radii up to the nearest integer value) and the components physical values (such as capacitance in the course of the IPU design). Namely, the peak power of the manufactured IPU is about 92% of the calculated one, and the power drop is even less than the calculated value (18.7% as opposed to the 20%).

Several more general conclusions can be derived from these results. Low-frequency links tend to be more stable for the given parameters including r_{outR}. It is also interesting that in low-frequency cases the inner radii of the coils were significantly larger. The r_{inT}/r_{outR} ratio was in the range $0.4 \ldots 0.6$. For the high-frequency cases it was about 0.1 and lower. It is also can be said that the thinly distributed windings ensure higher stability of the inductive links.

The developed algorithm should be implemented for the IPU operated in the overcoupled mode. In this case, the output power is beyond the permissible minimum in the absence or small lateral misalignments, when the axial distance is less than the initial value. Thus, the minimal possible value of the axial distance must be chosen as initial value for optimization procedure. Also, the maximal value of the lateral misalignment should be set slightly higher than the expected one.

It should be noted, that the geometry optimization is a reliable solution and thus it is of special interest for biomedical applications. At the same time, it has its own limitations. So, presented algorithm can be considered as a first step in the design of a reliable and effective IPU.

REFERENCES

[1] R. Shadid and S. Noghanian, "A literature survey on wireless power transfer for biomedical devices," *Int. J. Antennas Propag.*, vol. 2018, Apr. 2018, Art. no. 4382841. [Online]. Available: https://www.hindawi.com/journals/ijap/2018/4382841/

[2] K. Agarwal, R. Jegadeesan, Y.-X. Guo, and N. V. Thakor, "Wireless power transfer strategies for implantable bioelectronics," *IEEE Rev. Biomed. Eng.*, vol. 10, pp. 136–161, 2017.

[3] K. N. Bocan and E. Sejdić, "Adaptive transcutaneous power transfer to implantable devices: A state of the art review," *Sensors*, vol. 16, no. 3, p. E393, Mar. 2016.

[4] A. B. Amar, A. B. Kouki, and H. Cao, "Power approaches for implantable medical devices," *Sensors*, vol. 15, no. 11, pp. 28889–28914, 2015.

[5] B. Lenaerts and R. Puers, *Omnidirectional Inductive Powering for Biomedical Implants*. Berlin, Germany: Springer, 2009, pp. 1–12.

[6] M. A. Hannan, S. Mutashar, S. A. Samad, and A. Hussain, "Energy harvesting for the implantable biomedical devices: Issues and challenges," *Biomed. Eng. OnLine*, vol. 13, no. 1, p. 79, Dec. 2014.

[7] A. Yakovlev, S. Kim, and A. Poon, "Implantable biomedical devices: Wireless powering and communication," *IEEE Commun. Mag.*, vol. 50, no. 4, pp. 152–159, Apr. 2012.

[8] J. S. Ho and A. S. Y. Poon, "Energy transfer for implantable electronics in the electromagnetic midfield," *Prog. Electromagn. Res.*, vol. 148, pp. 151–158, May 2014.

[9] B. S. Wilson and M. F. Dorman, "Cochlear implants: Current designs and future possibilities," *J. Rehabil. Res. Dev.*, vol. 45, no. 5, pp. 695–730, Dec. 2008.

[10] F.-G. Zeng, S. Rebscher, W. Harrison, X. Sun, and H. Feng, "Cochlear implants: System design, integration, and evaluation," *IEEE Rev. Biomed. Eng.*, vol. 1, pp. 115–142, 2008.

[11] R. B. North, "Neural interface devices: Spinal cord stimulation technology," *Proc. IEEE*, vol. 96, no. 7, pp. 1108–1119, Jul. 2008.

[12] P. Eldridge, B. A. Simpson, and J. Gilbart, "The role of rechargeable systems in neuromodulation," *Eur. Neurological Rev.*, vol. 6, no. 3, p. 187, 2011.

[13] J. D. Weiland and M. S. Humayun, "Visual prosthesis," *Proc. IEEE*, vol. 96, no. 7, pp. 1076–1084, Jul. 2008.

[14] M. A. Lebedev and M. A. L. Nicolelis, "Brain–machine interfaces: Past, present and future," *Trends Neurosci.*, vol. 29, no. 9, pp. 536–546, Sep. 2006.

[15] R. Baumgart, P. Thaller, S. Hinterwimmer, M. Krammer, T. Hierl, and W. Mutschler, "A fully implantable, programmable distraction nail (fitbone)—New perspectives for corrective and reconstructive limb surgery," in *Practice of Intramedullary Locked Nails*. Dordrecht, The Netherlands: Springer, 2006, pp. 189–198.

[16] G. Bergmann, F. Graichen, J. Dymke, A. Rohlmann, G. N. Duda, and P. Damm, "High-tech hip implant for wireless temperature measurements in vivo," *PLoS ONE*, vol. 7, no. 8, Aug. 2012, Art. no. e43489.

[17] J. X. Wang, J. R. Smith, and P. Bonde, "Energy transmission and power sources for mechanical circulatory support devices to achieve total implantability," *Ann. Thoracic Surg.*, vol. 97, no. 4, pp. 1467–1474, Apr. 2014.

[18] A. A. Danilov, G. P. Itkin, and S. V. Selishchev, "Progress in methods for transcutaneous wireless energy supply to implanted ventricular assist devices," *Biomed. Eng.*, vol. 44, no. 4, pp. 125–129, Nov. 2010.

[19] M. S. Slaughter and T. J. Myers, "Transcutaneous energy transmission for mechanical circulatory support systems: History, current status, and future prospects," *J. Cardiac Surg.*, vol. 25, no. 4, pp. 484–489, Jul. 2010.

[20] A. A. Danilov, E. A. Mindubaev, and S. V. Selishchev, "Methods for compensation of coil misalignment in systems for inductive transcutaneous power transfer to implanted medical devices," *Biomed. Eng.*, vol. 51, no. 1, pp. 56–60, May 2017.

[21] S. M. Abbas, M. A. Hannan, S. A. Samad, and A. Hussain, "Inductive coupling links for lowest misalignment effects in transcutaneous implanted devices," *Biomed. Eng./Biomedizinische Technik*, vol. 59, no. 3, pp. 257–268, Jun. 2014.

[22] A. A. Danilov and E. A. Mindubaev, "Influence of angular coil displacements on effectiveness of wireless transcutaneous inductive energy transmission," *Biomed. Eng.*, vol. 49, no. 3, pp. 171–173, Sep. 2015.

[23] K. J. Dormer, R. E. Nordquist, G. L. Richard, and J. V. D. Hough, "The use of rare-earth magnet couplers in cochlear implants," *Laryngoscope*, vol. 91, no. 11, pp. 1812–1820, Nov. 1981.

[24] J. C. Schuder, "Powering an artificial heart: Birth of the inductively coupled-radio frequency system in 1960," *Artif. Organs*, vol. 26, no. 11, pp. 909–915, Nov. 2002.

[25] E. Okamoto, Y. Yamamoto, Y. Akasaka, T. Motomura, Y. Mitamura, and Y. Nosé, "A new transcutaneous energy transmission system with hybrid energy coils for driving an implantable biventricular assist device," *Artif. Organs*, vol. 33, no. 8, pp. 622–626, Aug. 2009.

[26] S. M. Mehta, W. E. Pae, Jr., G. Rosenberg, A. J. Snyde, W. J. Weiss, J. P. Lewis, D. J. Frank, J. J. Thompson, and W. S. Pierce, "The LionHeart LVD-2000: A completely implanted left ventricular assist device for chronic circulatory support," *Ann. Thoracic Surg.*, vol. 71, no. 3, pp. S156–S161, Mar. 2001.

[27] T. Ozeki, T. Chinzei, Y. Abe, I. Saito, T. Isoyama, S. Mochizuki, M. Ishimaru, K. Takiura, A. Baba, T. Toyama, and K. Imachi, "Functions for detecting malposition of transcutaneous energy transmission coils," *ASAIO J.*, vol. 49, pp. 469–474, Jul. 2003.

[28] J. Friedmann, F. Groedl, and R. Kennel, "A novel universal control scheme for transcutaneous energy transfer (TET) applications," *IEEE J. Emerg. Sel. Topics Power Electron.*, vol. 3, no. 1, pp. 296–305, Mar. 2015.

[29] L. Hu, F. Yang, R. Xiaodong, X. Haibo, and F. Xin, "Detecting malposition of coil couple for transcutaneous energy transmission," *ASAIO J.*, vol. 62, no. 1, pp. 56–62, Jan./Feb. 2016.

[30] W. Han, K. T. Chau, C. Jiang, and W. Liu, "Accurate position detection in wireless power transfer using magnetoresistive sensors for implant applications," *IEEE Trans. Magn.*, vol. 54, no. 11, pp. 1–5, Nov. 2018.

[31] W.-Q. Niu, J.-X. Chu, W. Gu, and A.-D. Shen, "Exact analysis of frequency splitting phenomena of contactless power transfer systems," *IEEE Trans. Circuits Syst. I, Reg. Papers*, vol. 60, no. 6, pp. 1670–1677, Jun. 2013.

[32] A. Kurs, A. Karalis, R. Moffatt, J. D. Joannopoulos, P. Fisher, and M. Soljačić, "Wireless power transfer via strongly coupled magnetic resonances," *Science*, vol. 317, no. 5834, pp. 83–86, Jul. 2007.

[33] D. C. Galbraith, M. Soma, and R. L. White, "A wide-band efficient inductive transdennal power and data link with coupling insensitive gain," *IEEE Trans. Biomed. Eng.*, vol. BME-34, no. 4, pp. 265–275, Apr. 1987.

[34] A. A. Danilov, E. A. Mindubaev, and S. V. Selishchev, "Space-frequency approach to design of displacement tolerant transcutaneous energy transfer system," *Prog. Electromagn. Res. M*, vol. 44, pp. 91–100, 2015.

[35] B. H. Waters, A. P. Sample, P. Bonde, and J. R. Smith, "Powering a ventricular assist device (VAD) with the free-range resonant electrical energy delivery (FREE-D) system," *Proc. IEEE*, vol. 100, no. 1, pp. 138–149, Jan. 2012.

[36] P. Si, A. P. Hu, S. Malpas, and D. Budgett, "A frequency control method for regulating wireless power to implantable devices," *IEEE Trans. Biomed. Circuits Syst.*, vol. 2, no. 1, pp. 22–29, Mar. 2008.

[37] M. Schormans, V. Valente, and A. Demosthenous, "Frequency splitting analysis and compensation method for inductive wireless powering of implantable biosensors," *Sensors*, vol. 16, no. 8, 2016, Art. no. E1229.

[38] B. Larsson, H. Elmqvist, L. Rydén, and H. Schüller, "Lessons from the first patient with an implanted pacemaker:1958–2001," *Pacing Clin. Electrophys.*, vol. 26, no. 1, pp. 114–124, Jan. 2003.

[39] B. Pelletier, S. Spiliopoulos, T. Finocchiaro, F. Graef, K. Kuipers, M. Laumen, D. Guersoy, U. Steinseifer, R. Koerfer, and G. Tenderich "System overview of the fully implantable destination therapy—ReinHeart-total artificial heart," *Eur. J. Cardio-Thoracic Surg.*, vol. 47, no. 1, pp. 80–86, Sep. 2014.

[40] C. M. Zierhofer and E. S. Hochmair, "Geometric approach for coupling enhancement of magnetically coupled coils," *IEEE Trans. Biomed. Eng.*, vol. 43, no. 7, pp. 708–714, Jul. 1996.
[41] U.-M. Jow and M. Ghovanloo, "Design and optimization of printed spiral coils for efficient transcutaneous inductive power transmission," *IEEE Trans. Biomed. Circuits Syst.*, vol. 1, no. 3, pp. 193–202, Sep. 2007.
[42] A. A. Danilov, E. A. Mindubaev, and S. V. Selishchev, "Design and evaluation of an inductive powering unit for implantable medical devices using GPU computing," *Prog. Electromagn. Res. B*, vol. 69, pp. 61–73, 2016.
[43] V. T. Krasteva, S. P. Papazov, and I. K. Daskalov, "Magnetic stimulation for non-homogeneous biological structures," *Biomed. Eng. Online*, vol. 1, no. 1, p. 3, Dec. 2002.
[44] L. Ahma, M. Ibrani, and E. Hamiti, "Computation of SAR distribution in a human exposed to mobile phone electromagnetic fields," in *Proc. Prog. Electromagn. Res. Symp.*, vol. 2, 2010, pp. 1555–1557. [Online]. Available: https://www.researchgate.net/publication/287006227_Computation_of_SAR_distribution_in_a_human_exposed_to_mobile_phone_electromagnetic_fields
[45] O. Knecht, R. Bosshard, J. W. Kolar, and C. T. Starck, "Optimization of transcutaneous energy transfer coils for high power medical applications," in *Proc. IEEE 15th Workshop Control Modeling Power Electron. (COMPEL)*, Santander, Spain, Jun. 2014, pp. 1–10.

ARSENY A. DANILOV received the B.S. and M.S. degrees in electronic engineering and the Ph.D. degree in physics and mathematics from the National Research University of Electronic Technology, Moscow, Russia, in 2002, 2004, and 2007, respectively.

He is currently the Head of the Laboratory of Wireless Biomedical Interfaces, Institute of Biomedical Systems, National Research University of Electronic Technology, and a Senior Researcher with the Institute for Bionic Technologies and Engineering, Sechenov First Moscow State Medical University, Moscow, Russia. He has authored and coauthored about 50 papers. His main fields of activity are the design of implantable medical devices and investigation of the interaction between biological tissues and electromagnetic fields and waves. He is the Deputy Editor-in-Chief of the Russian journal *Meditsynskaya Tekhnika*, which is translated and published in English under the title *Biomedical Engineering*.

RAFAEL R. AUBAKIROV received the B.S. degree in electronic engineering from the National Research University of Electronic Technology, Moscow, Russia, in 2017, where he is currently pursuing the master's degree. He has authored one journal article and several conference papers. His current research interests include optimization algorithms, numerical modeling, and wireless energy transfer for implants.

EDUARD A. MINDUBAEV (M'16) received the B.S., M.S., and Ph.D. degrees from the National Research University of Electronic Technology, Moscow, Russia, in 2011, 2013, and 2018, respectively, all in engineering.

He is currently an Engineer with the Institute for Bionic Technologies and Engineering, Sechenov First Moscow State Medical University, Moscow, and an Assistant with the Institute of Biomedical Systems, National Research University of Electronic Technology. He has authored and coauthored about 40 technical papers. His research interests include wireless energy transfer, mechanical circulatory support systems, and implantable medical devices.

KONSTANTIN O. GUROV received the B.S. and M.S. degrees in electronic engineering from the National Research University of Electronic Technology, Moscow, Russia, in 2016 and 2018, respectively, where he is currently a Research Engineer. He has authored two journal articles and several conference papers about the problems of transcutaneous energy transfer, which is his main scientific interest.

DMITRY V. TELYSHEV received the B.S., M.S., and Ph.D. degrees from the National Research University of Electronic Technology, Moscow, Russia, in 2006, 2008, and 2011, respectively, all in electronic engineering.

He is currently the Director of the Institute for Bionic Technologies and Engineering, Sechenov First Moscow State Medical University, Moscow, Russia, and an Associate Professor with the Institute of Biomedical Systems, National Research University of Electronic Technology. He has authored and coauthored about 70 technical papers. His research interests include the design of mechanical circulatory support systems, recording and processing of ECG, and general problems of design of implantable medical devices.

SERGEY V. SELISHCHEV (M'99–SM'17) received the Dipl.-Ing. from the National Research University of Electronic Engineering, Moscow, Russia, in 1976, the Ph.D. degree in physics and mathematics from the Institute of Metallurgy and Material Sciences of Russian Academy of Sciences, in 1983, and the Dr.-Sc. degree in physics and mathematics from the Institute of Thermophysics of Russian Academy of Sciences, in 1988. He is currently the Director of the Institute of Biomedical Systems, National Research University of Electronic Technology.

In 1993, he has initiated the teaching of biotechnical and medical devices and systems at the National Research University of Electronic Technology. In 1999, he has founded the Department of Biomedical Systems (since 2018 undergoing as the Institute of Biomedical Systems) at this institution and chaired it since foundation. He was a Project Leader in the development of the first Russian automated defibrillator and the first Russian ventricular assist device, namely, Sputnik. He has authored and coauthored more than 200 scientific and technical papers. He is also an Editor-in-Chief of the Russian journal *Meditsynskaya Tekhnika*, which is translated and published in English under the title *Biomedical Engineering*.